Article

A cost-effective force field tailored for solid-phase simulations of OLEDs materials

Mónica Moral, Wonjoon Son, Yoann Olivier, Juan-Carlos Sancho-García, and Luca Muccioli

J. Chem. Theory Comput., **Just Accepted Manuscript** • DOI: 10.1021/acs.jctc.5b00164 • Publication Date (Web): 12 Jun 2015

A cost-effective force field tailored for solid-phase simulations of OLEDs materials

M. Moral,[†] W.-J. Son,[‡] J. C. Sancho-García,[†] Y. Olivier,[¶] and L. Muccioli[*,§,‖]

Departamento de Química Física, Universidad de Alicante, 03080 Alicante, Spain, Samsung Advanced Institute of Technology, Suwon, 443-803 Gyeonggi-do, South Korea, Laboratory for Chemistry of Novel Materials, University of Mons, 7000 Mons, Belgium, Department of Industrial Chemistry "Toso Montanari", University of Bologna, 40136 Bologna, Italy, and Laboratoire de Chimie des Polymères Organiques (LCPO), UMR 5629, University of Bordeaux, 33607 Pessac, France

E-mail: Luca.Muccioli@u-bordeaux.fr

Abstract

A united atom force field is empirically derived by minimizing the difference between experimental and simulated crystal cells and melting temperatures for eight compounds representative of organic electronic materials used in OLEDs and other devices: biphenyl, carbazole, fluorene, 9,9'-(1,3-Phenylene)bis(9H-carbazole) 1,3-bis(N-carbazolyl)benzene (mCP), 4,4′- Bis(N-carbazolyl)-1,1′-biphenyl (pCBP), phenazine, phenylcarbazole, and triphenylamine. The force field is verified against dispersion-corrected DFT calculations and shown to successfully reproduce the crystal struc-

[*]To whom correspondence should be addressed
[†]Departamento de Química Física, Universidad de Alicante, 03080 Alicante, Spain
[‡]Samsung Advanced Institute of Technology, Suwon, 443-803 Gyeonggi-do, South Korea
[¶]Laboratory for Chemistry of Novel Materials, University of Mons, 7000 Mons, Belgium
[§]Department of Industrial Chemistry "Toso Montanari", University of Bologna, 40136 Bologna, Italy
[‖]Laboratoire de Chimie des Polymères Organiques (LCPO), UMR 5629, University of Bordeaux, 33607 Pessac, France

ture also for two larger compounds employed as hosts in phosphorescent and thermally activated delayed fluorescence OLEDs: N,N′-Di(1-naphthyl)- N,N′-diphenyl-(1,1′-biphenyl)- 4,4′-diamine (NPD), 1,3,5-tri(1-phenyl-1H-benzo[d]imidazol-2-yl)phenyl (TPBI).

The good performances of the force field, coupled to the large computational saving granted by the united atom approximation, make it an ideal choice for the simulation of the morphology of emissive layers for OLED materials in crystalline or glassy phases.

1 Introduction

Molecular and polymeric materials composed by recurrent aromatic moieties, such as phenyl and carbazolyl, are becoming ubiquitous in organic electronics applications:[1] as donors and acceptors for organic solar cells,[2,3] metal-free dyes[4,5] or hole transporters[6] in Graetzel solar cells, host semiconducting[7–12] and emitting materials in organic light-emitting diodes (OLEDs),[9,13–17] to name the most important ones. In particular all the emissive, hole and electron conducting (blocking) layers in small molecule and polymer OLEDs are often composed by nitrogen-rich units featuring a sp^2 or sp^3-hybridized nitrogen (e.g. carbazoles and amines).[7,18]

To rationally improve the efficiency of the emissive layer, in particular to gain insight into the interplay between the host and guest electronic structures and consequently access to the rates governing hole-electron recombination and light emission processes, atomistic-like simulations combined with quantum chemistry calculations represent the most powerful theoretical method currently available.[19,20] However, high computational costs associated with such methodologies prevented so far their application to the chemically detailed simulation of an OLED, which are typically modeled only at macroscopic[21] or lattice level.[22,23]

Indeed, to investigate microscopically how structure affects kinetic and energetic magnitudes determining the efficiency in organic electronic devices, it is urgent to derive and employ force fields not only reliably reproducing the physical properties of these materials, but also simple

and efficient enough to grant the possibility of simulating the morphology of a whole emissive layer,[19,20,24,25] i.e. of samples with dimensions of about $10^4 - 10^6$ nm^3. Note that the most popular ones are optimized for other purposes[26] and that, to date, the literature appears to be not only scarce of efforts for obtaining the first objective, exception made for the notable work of Andrienko, Lennartz, Wenzel and collaborators,[19,20,24,27–30] but also almost absent of attempts of reducing the computational cost via the derivation of simpler potentials.

In the following, we thus try to partially fill this gap by describing and tailoring a simple and computationally cost-effective united atom force field, able to reproduce rather accurately the solid phase properties of some typical organic compounds employed in OLED industry (Figure 1). The investigation is particularly timely because of the rise, besides transition metal-based phosphorescent emitters, of new all-organic ones with thermally activated[12,13,31–35] and aggregation induced fluorescence[14–16,36] playing a major role, that are going to consent the realization of fully organic OLEDs, and represents the ideal prosecution of our previous study on the accurate theoretical calculation of singlet-triplet energy gaps for this class of materials.[34]

2 Molecules and force field initial setup

We started by selecting eight small molecules of known crystal cell structure, shown in Figure 1: biphenyl (BPH), carbazole (CBZ), fluorene (FLU), 1,3-bis(carbazol-9-yl)benzene (mCP), 4,4′-dicarbazole-1,1′-biphenyl (CBP), phenazine (PHE), phenylcarbazole (PCZ) and triphenylamine (TPA)[37]. All these molecules are either used as host OLED materials themselves (e.g. PCZ , TPA, CBP), or constitute recurring chemical units in more complex polymeric or molecular structures.[18,38] We then proceeded to the setup of a united atom (UA) force field able to adequately reproduce the crystal structure of the selected compounds. The choice of a UA representation, also known as "extended atom" approximation, is justified by the large saving of computational time it allows, at the cost of a minimal loss of accuracy and of some

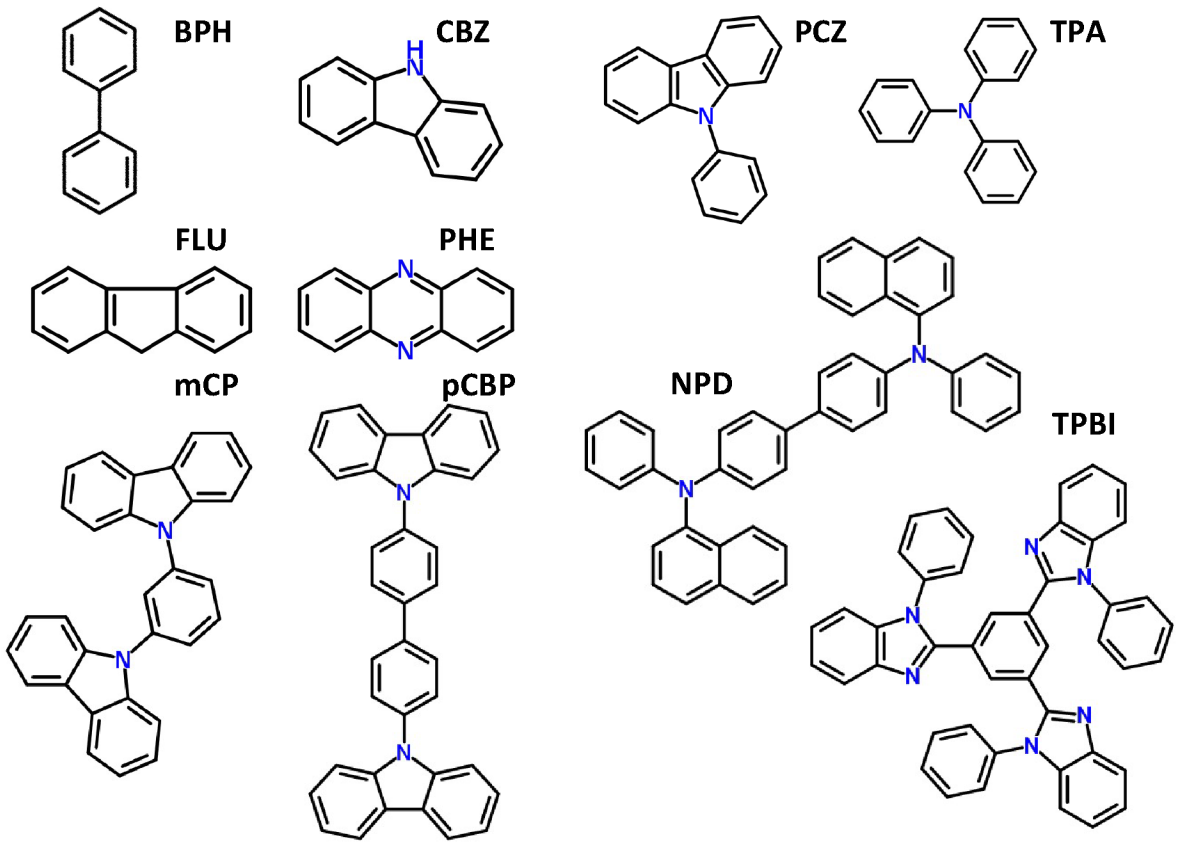

Figure 1: Chemical structures of the compounds studied: biphenyl (BPH), carbazole (CBZ), fluorene (FLU), 9,9'-(1,3-Phenylene)bis(9H-carbazole) 1,3-bis(N-carbazolyl)benzene (mCP), 4,4′-Bis(N-carbazolyl)-1,1′-biphenyl (pCBP), phenazine (PHE) 9-Phenyl-9H-carbazole (PCZ), and triphenylamine (TPA) compose the training set used for the empirical parameterization, while N,N′-Di(1-naphthyl)-N,N′-diphenyl-(1,1′-biphenyl)-4,4′-diamine (NPD), 1,3,5-tri(1-phenyl-1H-benzo[d]imidazol-2-yl)phenyl (TPBI) were simulated only to test the optimized version of the force field. The H atoms and the corresponding C–H bonds are omitted for clarity.

extra effort in its parameterization.[39] In a nutshell, every aliphatic or aromatic hydrogen atom is modelled only implicitly[40] and its mass is summed to the one of carbon atom it is bonded to. Such a customization of the force field can indeed turn into a long exercise requiring several steps.[41] Here we started with adopting the widely used AMBER-like or CHARMM-like potential energy function:[42]

$$\begin{aligned} U_{\text{total}} \quad = \quad & \sum_{\text{bonds}} K_r^*(r - r_e^*)^2 + \sum_{\text{angles}} K_\theta^*(\theta - \theta_e^*)^2 + \\ & \sum_{\text{dihed}} \sum_{n^*} V_n^* \left[1 + \cos(n^*\phi + \gamma_n^*)\right] + \sum_{\text{improper}} K_\phi^*(\phi - \phi_e^*)^2 + \\ & \sum_{\text{atoms}} \left\{ 4\sqrt{\epsilon_i^* \epsilon_j^*} \left[\left(\frac{\sigma_i^* + \sigma_j^*}{2r_{ij}} \right)^{12} - \left(\frac{\sigma_i^* + \sigma_j^*}{2r_{ij}} \right)^{6} \right] + \frac{q_i^* q_j^*}{r_{ij}} \right\}. \end{aligned} \tag{1}$$

where for clarity all the parameters have been starred. For the harmonic constants K_r and K_θ we rely on the AMBER95 parameter set,[43] while the corresponding equilibrium distances and angles r_e and θ_e where adjusted comparing the equilibrium molecular mechanics geometries with the ones produced by highly accurate calculations. The torsional parameters V_n, n, γ_n were borrowed from the AMBER95 dataset for what concerns the rigid ones, e.g. torsions involving carbon atoms belonging to the same aromatic ring, while soft, anharmonic torsions were here parametrized with quantum chemistry calculations[29,41,44] at PBE0-D3(BJ)/def2-TZVP level. In practice, only three types of torsion were reworked: phenyl-phenyl, phenyl-carbazole, and the improper torsion involving the out-of-plane vibration of sp^2 nitrogen; the phenyl-nitrogen torsion in TPA being modeled with standard parameters, as it is dominated by steric repulsion which confers it a propeller-like structure.[45] Fully relaxed scans of the potential energy surface as a function of the dihedral angle were run in steps of 5 degrees, using BPH and PCZ as target fragments, with the obtained profiles shown in Figure 2. It is worth noting that these torsions are present also in the largest compounds of the training set, namely mCP and pCBP, and in many other OLED materials.[18,38]

The force field parameters matching the torsional potentials were optimized with the pro-

cedure described in reference,[44] consisting in deriving the free energy torsional profile with adaptive biasing force MD runs[46] and fitting the difference between QM and MD with a cosine series (see eq 1). Turning to the Lennard-Jones (LJ) parameters σ_i and ϵ entering the last term of eq 1, nine atom types were first identified (i. e. chemically equivalent atoms sharing the same parameters, see Tables 1 and 2) and their initial values was set to the one found in literature references.[43,47–49] As it is customarily done,[42,50] the atomic charges q were derived by fitting the molecular electrostatic potential obtained by quantum chemistry calculations. For this purpose the PBE0-D3(BJ)/def2-TZVP model chemistry was adopted,[51–55] with numerical thresholds systematically increased with respect to defaults, and dispersion corrections -D3(BJ),[56] because as we have reported recently, it shows good all-around performances for some of the compounds studied here, as well as for some emitters exhibiting thermally activated delayed fluorescence (see reference[34] for further details). Molecular geometries were first optimized by PBE0/def2-TZVP calculations, and then the charges on the heavy atoms were calculated at PBE0/TZVP level with the electrostatic potential fitting algorithm[57] implemented in the GAUSSIAN09 package.[58] All the other quantum mechanics calculations were performed with the ORCA code, version 3.0.0.[59] All the atomistic simulations were run with the NAMD 3.0 software.[60] The trajectories were analyzed with a in-house written Fortran 95 code.

Table 1: Atom types included in the force field and their occurrence for each molecule of the training set.

name	description	BPH	CBZ	FLU	mCP	pCBP	PHE	PCZ	TPA
C2	-CH_2- group	-	-	1	-	-	-	-	-
CA	aromatic C	-	2	2	4	4	4	4	-
CH	ua aromatic C-H group	10	8	8	16	28	8	11	15
CX	bridge aromatic C	2	2	2	4	6	-	-	-
CY	aromatic C bonded to sp^2 N	-	-	-	2	2	-	1	3
N	aromatic sp^2 N	-	-	-	-	-	2	-	-
NH	carbazole NH group	-	1	-	-	-	-	-	-
N3	sp^2 N (e.g. in PCZ)	-	-	-	2	2	-	1	-
N4	triphenylamine sp^3 N	-	-	-	-	-	-	-	1

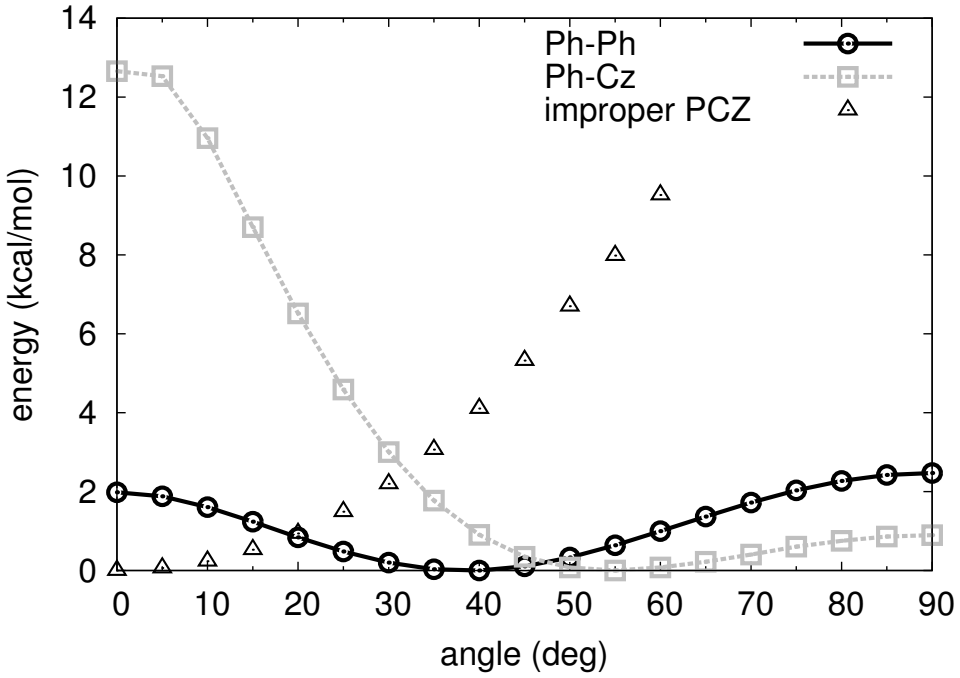

Figure 2: Quantum mechanical potential for the phenyl-phenyl dihedral angle in BPH (circles), for the phenyl-carbazole dihedral angle in PCZ (squares), and for the improper dihedral carbazole-N-phenyl in PCZ (triangles), systematically calculated at the PBE0-D3(BJ)/def2-TZVP level[34] by fully relaxing the geometry while keeping fixed the dihedral angle.

Table 2: Starting values of Lennard-Jones parameters σ (Å) and ϵ (kcal/mol) for each atom type and corresponding reference ("start" force field), and percentage variation of the radii σ for the heuristic R1, R2, and R3 force fields.

name	σ	ϵ		R1	R2	R3
C2	3.70	0.1094	[48]	+10%	+10%	+10%
CA	3.43	0.0860	[50]	+2%	+4%	+4%
CH	3.56	0.1114	[49]	+3%	+4%	+4%
CX	3.43	0.0860	[50]	-	-4%	-4%
CY, CW	3.43	0.0860	[50]	+4%	+4%	+5%
N	3.28	0.1700	[50]	+5%	+4%	-
NH	3.28	0.1700	[50]	+5%	+4%	+4%
N3	3.28	0.1700	[50]	+5%	+4%	+4%
N4, N5[61]	3.28	0.1700	[50]	+5%	+4%	-

3 Computational strategy

For each target compound, a supercell was created by replicating the experimental crystal cell along its axes a, b, c, to have thus at least three replica per side, and supercell sides the closest possible to 5 nm, in order to realize a sensible compromise betweeen finite size effects and computational costs. With these criteria, the sample sizes range from approximately 6000 to 10000 atoms, corresponding to N=540 (BPH, 6 x 9 x 5 supercell[62]), 756 (CBZ, 7 x 3 x 9[63]), 756 (FLU 7 x 3 x 9[64]), 288 (mCP, 6 x 4 x 3[65]), 180 (pCBP, 6 x 3 x 5[66]), 560 (PHE, 7 x 10 x 4[67]), 360 (PCZ, 3 x 5 x 3[68]), and 432 (TPA, 3 x 3 x 3[69]) molecules per simulation box, respectively. For each parameter set, supercells were equilibrated with Molecular Dynamics at constant volume for 0.4 ns, then at atmospheric pressure for 2 ns, and finally density and box sizes were averaged over a further 1 ns-long run; the simple velocity scaling thermostat and Berendsen's barostat were used in all the runs. Simulated temperatures for each compound correspond to the ones of the measurement of experimental crystal structure as downloaded from the Cambridge Structural Database (CSD, entries BIPHEN04, CRBZOL04, FLUREN01, NEPWUB, KANYUU, PHENAZ04, PEMWEJ, ZZZJCQ01), typically room temperature (set to 293 K for BPH, FLU, PHE, PCZ, TPA) or below (168 K CBZ, 291 K mCP, 120 K pCBP), while the pressure is always fixed to 1 atm.

In order to be able to quantitatively compare the results of two different force fields, and eventually to systematically vary the FF parameters to match the experimental results, it is necessary to define an appropriate scoring function. Here, the deviation of the simulated cell from the experimental one was measured as

$$\mathrm{F} \quad = \quad \frac{1}{2} \left(\Delta_{vol} \; + \; \Delta_{def} \right) \tag{2}$$

which accounts, through the function Δ_{vol}, for the variation of the volume of the simulated cell (subscript s) with respect to the experimental one (subscript e), and for the deformation

of the cell shape through Δ_{def}:

$$\Delta_{vol} = \frac{1}{3}\frac{|V_e - V_s|}{V_e} \quad (3)$$

$$\Delta_{def} = \frac{1}{3}\left[\prod |\cos(\delta_e^i - \delta_s^i)|^{-1} \prod \left(1 + \frac{|l_e^i - l_s^i|}{l_e^i}\right) - 1\right] \quad (4)$$

where $l^i = a,\ b,\ c$ and $\delta^i = \alpha,\ \beta,\ \gamma$ are the crystal cell axes and angles, respectively, and $V = abc\sqrt{1 - \cos^2\alpha - \cos^2\beta - \cos^2\gamma + 2\cos\alpha\cos\beta\cos\gamma}$ is the volume of the crystal unit cell. In order not to bias the scoring functions towards systems with smaller unit cells, for which the absolute variations of volume and cell sides are obviously smaller, both Δ_{vol} and Δ_{def} are dimensionless quantities. In practice, F is zero for a perfect agreement between experiment and simulation, is greater than zero otherwise, and for the simple case of an isotropic deformation of the experimental cell (i. e. $l_s^i = \lambda\ l_e^i$), takes the value of $|\lambda - 1|$ for $\lambda \to 0$; hence, small values of F can be assimilated to the strain of the simulated cell with respect to the experimental one.[70]

4 Optimization of Lennard-Jones radii

In a classical force field, the intermolecular forces responsible for the cohesive energy in crystal phase are represented by a Lennard-Jones and an electrostatic term - see last summation in eq 1. Considering that atomic point charges are directly derived from DFT calculations, which are accurate enough in the description of the molecular charge density,[71] our empirical exploration was limited to optimizing the Lennard-Jones parameters (ϵ and σ, see also Tables 1 and 2), that conversely are very difficult to evaluate accurately by purely theoretical means.[72,73]

With the initial parameter set taken from the literature and customized with QM charges and dihedrals, an average score of 0.027 is obtained, a rather unsatisfactory value as it translates in overestimations of the densities as large as 0.12 g/cm^3 with the exception of BPH.

The observation of BPH being an outlier, which is confirmed for almost all the attempted parameterizations, it is not surprising as it is known that the intermolecular interactions for benzene and short oligophenyls are particulary difficult to model with classical, non polarizable force fields[74] and special parameters are often required to obtain good accuracy.[75,76] In addition, the united atom approximation, that eliminates the aliphatic hydrogens and their point charges, yielded to a poor description of the electric quadrupoles of phenyl rings.[77]

Also the global overestimation of the densities with standard parameters can be easily rationalized, recalling that the OPLS LJ parameters are optimized for the simulation of liquids,[78] and not for the solid state. To support this statement with an example, it is worth noticing that the LJ parameters reported in Table 2 gave satisfactory results in modeling the liquid crystal phases of metal-free phthalocyanices,[79] while conversely they yield a rather poor description of poly-3-hexyl-thiophene crystalline domains.[80] Interestingly, a similar overestimation of the experimental density was observed for the latter system: in that case, the bias was corrected by increasing the σ of the aliphatic carbons of the hexyl chains by 8%.[80] Here we applied the same strategy: after having assessed that small variations of the various ϵ do not alter significantly the scoring function, as shown in Figure S1, we proceeded with a systematic increase of the atom sizes σ for the atom types in Table 1, starting from the most abundant ones (CA and CH).

From inspecting Figure 3 it can be appreciated how the strategy of progressively modifying the σ parameters is successful: while no improvement is obtained by decreasing σ for CA or CH, conversely an increase of 2-4 percent points significantly reduces the average score from the initial value of 0.027 to a more acceptable 0.018. It is also useful to observe in Figure 3 (see also Figures S1 and S2) that the most important contribution to the total score comes from the anisotropic deformation term Δ_{def}, which cannot be decreased as Δ_{vol} by uniformly scaling all the atom sizes. Therefore, once this stage of optimization was reached, we started from the "CH +4%"force field and applied some heuristic changes to the other atom types radii, by considering the relative occurrence of the atom types (Table 1) and

the separate scores of the different molecules in the training set (see Figure S2), obtaining three refined parameterizations, labeled R1, R2, R3, detailed in Table 2. These attempts further reduced the score, namely to a minimum of about 0.013 for the R3 case, that was accordingly selected as force field of election for further optimization. As shown in Table 3, with this parameterization all the simulated cell parameters and densities, BPH excluded, are very close to their experimental counterparts (RMSD 0.32, 0.16, and 0.43 Å for a, b, and c, and 0.026 g/cm^3 for density).

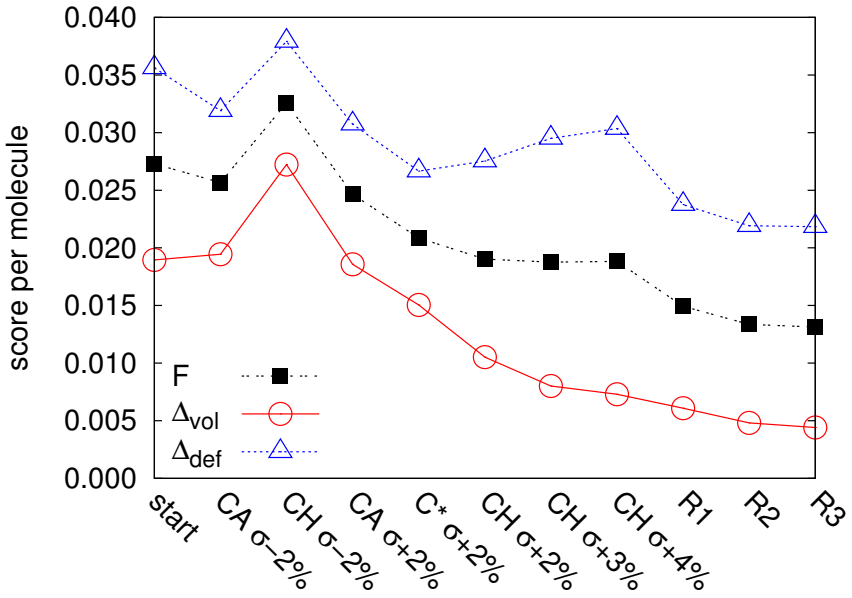

Figure 3: Performance of the different parameterizations obtained by varying the LJ radii. C* stands for all carbon atom types. R1, R2, R3 are further refinements of the "CH σ+4%" force field, as described in the text.

5 Tuning of Lennard-Jones potential well depths

Following the observation that the structure of the crystal cell is only weakly infuenced by changes of the potential well depth ϵ, in the previous section we tackled next the optimization of the σ parameters for reproducing accurately the experimental crystal structures. However, at this stage the ϵ values were left unoptimized, still demanding an alternative physical property for the purpose. With this purpose, we choose the melting points of the

Table 3: Experimental unit cells (e) and simulated ones (s) with the united atom R3 and R3 $\epsilon - 8\%$ force fields, and full atom FA (AMBER95 plus PBE0/def2-TZVP point charges) and T-FA force fields (identical to FA but with reparameterized dihedrals). Densities ρ are expressed in g/cm^3, cell volumes in Å^3, sides in Å, and angles in degrees. The angles, where equal to 90 degrees in the experimental cell, were kept fixed to this value during the simulation. The overall quality of the result is evaluated with the F score (eqs 2-4)

compound & FF		ρ	V	a	b	c	α	β	γ	$F \cdot 10^2$
BPH	e	1.18	435.8	8.12	5.63	9.51	90.0	95.1	90.0	0.0
R3	s	1.12	460.5	8.64	5.67	9.38	90.0	95.5	90.0	2.4
R3 $\epsilon - 8\%$	s	1.10	470.0	8.89	5.60	9.42	90.0	95.6	90.0	3.2
FA	s	1.14	451.1	8.62	5.40	9.67	90.0	95.3	90.0	2.6
T-FA	s	1.15	449.9	8.54	5.43	9.68	90.0	95.3	90.0	2.3
CBZ	e	1.36	818.5	7.63	18.93	5.66	90.0	90.0	90.0	0.0
R3	s	1.34	827.0	7.63	18.73	5.78	90.0	90.0	90.0	0.7
R3 $\epsilon - 8\%$	s	1.34	827.8	7.62	18.74	5.79	90.0	90.0	90.0	0.8
FLU	e	1.20	917.6	8.47	18.92	5.72	90.0	90.0	90.0	0.0
R3	s	1.21	917.3	8.31	18.72	5.89	90.0	90.0	90.0	1.0
R3 $\epsilon - 8\%$	s	1.20	923.6	8.34	18.75	5.90	90.0	90.0	90.0	1.1
mCP	e	1.26	2159.7	9.07	12.50	19.04	90.0	90.0	90.0	0.0
R3	s	1.26	2161.7	9.59	12.40	18.17	90.0	90.0	90.0	1.9
R3 $\epsilon - 8\%$	s	1.25	2168.2	9.60	12.39	18.22	90.0	90.0	90.0	2.0
pCBP	e	1.31	1314.1	8.01	16.01	10.24	90.0	110.2	90.0	0.0
R3	s	1.34	1293.3	8.16	16.03	9.88	90.0	111.4	90.0	1.2
R3 $\epsilon - 8\%$	s	1.34	1295.9	8.16	16.03	9.90	90.0	111.3	90.0	1.1
FA	s	1.20	1420.2	8.42	14.97	11.26	90.0	109.3	90.0	5.2
T-FA	s	1.29	1373.9	9.47	14.63	9.91	90.0	114.9	90.0	6.3
PHE	e	1.33	460.1	7.08	5.07	12.79	90.0	102.3	90.0	0.0
R3	s	1.32	463.8	6.73	5.09	13.51	90.0	101.1	90.0	0.2
R3 $\epsilon - 8\%$	s	1.31	466.2	6.74	5.12	13.48	90.0	101.1	90.0	2.1
PCZ	e	1.22	2887.0	14.53	10.98	18.09	90.0	113.5	90.0	0.0
R3	s	1.24	2861.8	14.88	10.64	18.07	90.0	114.1	90.0	1.1
R3 $\epsilon - 8\%$	s	1.23	2876.9	14.90	10.67	18.09	90.0	114.1	90.0	1.0
FA	s	1.15	3126.9	16.24	10.53	18.28	90.0	116.1	90.0	4.3
T-FA	s	1.22	2868.6	14.48	10.54	18.79	90.0	112.5	90.0	1.5
TPA	e	1.18	5512.2	15.66	22.26	15.81	90.0	90.0	91.0	0.0
R3	s	1.19	5485.4	15.64	22.18	15.81	90.0	90.0	91.0	0.1
R3 $\epsilon - 8\%$	s	1.18	5538.9	15.73	22.17	15.88	90.0	90.0	91.0	0.3
NPD	e	1.23	1691.9	10.30	11.33	14.49	82.4	77.7	75.6	0.0
R3 $\epsilon - 8\%$	s	1.26	1649.4	10.18	11.42	14.18	82.3	77.5	75.8	1.1
TPBI:CH_3-OH	e	1.25	3735.2	11.25	18.69	17.76	90.0	101.6	90.0	0.0
R3 $\epsilon - 8\%$	s	1.25	3722.2	11.01	18.23	18.54	90.0	100.9	90.0	1.6

target compounds, because they are a good indicator of intermolecular cohesion energy in the crystal, and attempted some scaling of the ϵ to maximize the agreement with experiment. A possible alternative would have been to choose boiling points, but the latter may not be available for the large compounds typically used in OLEDs, and in addition they are less relevant for OLED processing because often too high and far from room temperature. Melting points are straightforwardly determined with computer simulations by heating the crystal at increasing temperature until achieving the isotropic liquid phase, though hysteresis and system size may play an important role, typically leading to an overestimation of the actual melting temperature.[81,82] Here we used the supercells described in the previous sections as starting configurations, and equilibrated them for 3 ns at each simulated temperature and at atmospheric pressure. The temperature scan was performed at intervals of 25 K, typically starting at 300 K. As an operational definition of the melting point, the lowest temperature at which the sample becomes orientationally isotropic after 3 ns of simulation was considered. An example of the typical characterization of the phase change in terms of density, orientational order parameter, translational diffusion coefficient and radial distribution is reported in the Supporting Information.

Clearly this is just a coarse measurement that is expected to produce an overestimation of melting points, because the interval of 25 K is rather large and the sampling time of 3 ns may be too short for the process to occur at temperatures close to the melting point. Once melting points were estimated, the performance of each force field were evaluated by means of the absolute deviation between experimental and simulated ones ($|\Delta T| = \sum_{i=1}^{8} |T_e^{m,i} - T_s^{m,i}|/8$); on the basis of the previous considerations on the melting point determination, any value below 50 K can be considered a very good score. In attempting this evaluation, it is also important to take into account that there is no guarantee that a classical force field able to reproduce simulataneously the experimental melting point and the crystal structure may exist: for instance, it may occur that by altering the ϵ, also the crystal cell scoring function F could increase.

From Table 4, that resumes the scores for all the attempts of scaling ϵ parameters, we observe that luckily it is not the case for changes up to 10% with respect to the initial values, but that on the other hand the melting point are largely overestimated by the force fields. The scores also show that all the variations of the R3 force field proposed here overestimate the boiling points of the target molecules, with the usual exception of BPH. In order to decrease the boiling points, the interaction between atoms must be decreased, and hence ϵ reduced, but with the constraint of not worsening the reproduction of experimental crystal structure, monitored through the F scoring function. In our case, we found that the best compromise is obtained with a scaling to 92% of the original interaction strengths (Table 2), and we finally labelled this force field as "R3 $\epsilon - 8\%$". By examining again the results presented in Table 3, it can be noticed that the performances are slightly lower than the ones of R3, while the melting temperatures obtained for the scaled force field are at least 20 K closer to the experimental ones. Using this parameterization we also computed the surface energies for crystal (100), (010) and (001) planes, and for glassy samples obtained by freezing and equilibrating the liquid samples obtained above (see figure S5 and table S5 for further details). Such energies vary in a range between 0.05 and 0.15 J/m^2 for the crystal phase, in line with calculated[83,84] and experimental data[85] for other organic crystals. Conversely they are almost halved in glass phase (0.05-0.08 J/m^2), reflecting the lower internal energy of the bulk glass phase with respect to the bulk crystal.

6 Additional tests for the intermolecular potential

As a further quality check of R3 $\epsilon - 8\%$ force field, we compared its prediction for selected intermolecular potential energy curves with the ones produced by state-of-the-art dispersion-corrected Density Functional Methods (DFT) methods,[73] with the latter specifically including the correct dependence on the internuclear separation at large distances; i.e., the so-called long-range behavior. We selected for this purpose the well-rounded Perdew-Burke-Ernzerhof

Table 4: Melting points (K) for the studied compounds, as obtained by systematically rescaling the original LJ energy well depths ϵ of all atom types, and using the radii of the R3 parameter set. The corresponding crystal structure score F and the mean absolute deviation between experimental and simulated melting temperatures ($|\Delta T| = \sum_{i=1}^{8} |T_e^{m,i} - T_s^{m,i}|/8$, in K) are also reported.

compound	EXP[86]	R3	+10%	-5%	-8%	-10%	-15%	-20%
BPH	342	325	350	325	300	300	300	275
CBZ	518	700	750	675	675	650	625	600
FLU	386	550	600	525	525	500	500	475
mCP	449	725	775	700	700	700	650	650
pCBP	556	950	1050	900	875	850	825	775
PHE	447	650	675	625	600	600	575	550
PCZ	369	550	600	525	525	525	475	425
TPA	399	475	525	475	475	450	425	400
$\|\Delta T\|$	0	187	232	165	162	149	124	102
$F \cdot 10^2$	0	1.31	1.32	1.34	1.44	1.90	1.92	2.05

(PBE) functional in its standard hybrid (PBE0) and revised (revPBE0) versions[51–54] with the rather large (nearly-converged) def2-TZVP basis set, while regarding the dispersion corrections, we employed either the -D3(BJ) function[56] or the -NL (van der Waals) approach,[87] to separately disentangling the effect (if any) of both the functional form and the dispersion correction used. In addition, we tested the (computationally inexpensive compared to other DFT-based methods) recently developed HF-3c method, which includes Kruse and Grimme's geometric counterpoise corrections (gCP), the -D3(BJ) dispersion correction again, and a short-range basis incompleteness (SRB) correction for systematically overestimated bond lengths for electronegative elements when employing small basis sets.[88] The level of accuracy of the above theoretical methods was first verified by comparison with high level calculations published by Sherrill and coworkers by using accurate (nearly-converged) methods such as CCSD(T)/aug-cc-pVDZ, CCSD(T)/aug-cc-pVQZ, and MP2/aug-cc pVQZ, all of them including counterpoise correction (CP) to reduce as much as possible the well-known basis set incompleteness error typical of these calculations.[89] In particular, the classical cofacial and "T" geometries were explored for a pair of benzene molecules, and the corresponding intermolecular energies were calculated as function of the distance between the centers of

mass of the two interacting molecules (figure 4). PBE0 and revPBE0 give very similar energies, while the choice of the dispersion correction, -D3(BJ) or -NL, seems more critical, with -NL providing systematically weaker interaction energies with respect to -D3(BJ), and getting thus closer to the CCSD(T) reference values. HF-3c is in line with the more accurate methods for the T configuration, but instead largely overestimates the maximum interaction energy and underestimates the distance at which the cofacial interaction is maximum. This occurs also for PBE0 and revPBE0 calculations, for both benzene-benzene configurations, but to a much lower extent, though not negligible in terms of percentage, in particular for the energies (for all the values of "equilibrium" distances and energies, see additional tables S1-S4 in the supporting information). It can then be preliminarily concluded that for small aromatic molecules, dispersion-corrected PBE0/def2-TZVP calculations (independently of the correction used) give semiquantively accurate results for energies, and quantitative for distances, while the computationally cheaper HF-3c cannot be considered reliable enough, at least for π-stacking energies, like in the case of the benzene cofacial dimer.

We proceeded then to the evaluation of intermolecular energies for molecular pairs of BPH and TPA (see supporting information for PCZ), in this case comparing quantum chemistry calculations with molecular mechanics. These molecules, at their experimental geometry in the crystal phase, were rotated into their principal inertial frame and superimposed. One of them was kept fixed, while the second was moved along the three cartesian directions, corresponding to the orientation of the inertia axes with increasing eigenvalue. Starting with the extreme case of biphenyl (figure 5 left), we notice that all the quantum chemistry methods give approximately the same prediction for the minimum energy distance, while both the "start" and "R3 $\epsilon - 8\%$" provide a rather large underestimation (about 1 Å) for the x and y diplacement directions. The rationale of this behaviour can be found in the united atom approximation: as shown by the snapshots in figure 5 left, the x and y directions correspond to hydrogen-hydrogen contacts. These hydrogen are not present in the united atom force fields, where they are only partially compensated by a larger van der Waals radius on the

corresponding carbon, hence these force fields underestimate the distance, and overestimate the interaction. As a further proof, we computed the same potential energy also with the standard AMBER95/OPLS full atom parameters (black two-dashed lines), which conversely adheres to the ab initio curves. On the contrary, the z (π-stacking) direction is not affected by the united atom approximation, and here both "start" and "R3 ϵ8%" perfectly agree with DFT values, while as expected HF-3c, and more surprisingly AMBER95, overestimate the attraction between the two parallel BPH molecules. Moving to the larger and more isotropic TPA molecule, the curves in figure 5 right show that in this case united atom approximation is harmless and that the united atom FFs agrees with dispersion-corrected DFT values, while on the contrary HF-3c performs poorly, constantly overestimating the interaction energies. As a additional comment, it is worth noting that: i) the small differences between the "start" and "R3 ϵ8%" FFs results are always comparable or lower than the differences between one dispersion-corrected DFT calculation and another, and ii) the very similar performance of the two FFs for the computation of interaction potential curves contrasts with their different capabilities of reproducing the crystal cells of the target compounds. It rather appears from these results that for the time being, DFT-derived potential energy curves cannot be used as a reference method for parameterizing force fields,[90] and that the empirical tuning remains a more viable way.

For achieving a further validation of the "R3 $\epsilon - 8\%$" FF parameters, we repeated the simulation scheme described in section 3 for two molecules outside the training set for which the experimental crystal structure is known: N,N′-bis(1-Naphthyl)-N,N′-diphenyl-1,1′-biphenyl-4,4′-diamine (NPD, 5 x 4 x 3 supercell,[91] N=120 molecules, 5520 centers, CSD entry RE-HJAQ01) and 2,2′,2″-benzene-1,3,5-triyltris(1-phenyl-1H-benzimidazole) (TPBI, co-crystal with methanol, 4 x 3 x 3 supercell,[92] N=284 molecules for each species, 7776 centers, CSD entry QUCJAA). Again, wherever necessary, soft torsional potentials where re-parametrized (see figure S4), and united atom charges were calculated for each center for both molecules (see supporting information). In Table 3), it can be noticed that for these two example

molecules the quality of the reproduction of the experimental cells is good and comparable to the one achieved for the molecule belonging to the training set, suggesting that the Lennard-Jones parameters derived in this work could be safely transferred to other similar compounds.

To conclude, it is also worth assessing whether the parameterization exercise is just a consequence of opting for the united atom approximation, and also if this approximation is actually useful for saving precious computational time. For doing so, we chose the most complex molecule in the training set, pCBP, and set up a full atom force field by employing this time the full atom PBE0/def2-TZVP charges, and the popular GAFF parameters for Lennard-Jones and intramolecular parameters.[50] We produced two versions of this force field, one without re-optimizing the dihedral parameters (labelled FA in Table 3), and a second one (T-FA) where the phenyl-phenyl, phenyl-carbazole, and the improper sp2 nitrogen dihedrals were refined with ab initio data, exactly as described above for the united atom FF. As this re-optimization requires the simulation of BPH and CBZ as well, we reported in Table 3 also the results corresponding to their crystal cells. Starting with the difficult case of BPH, it appears that also the full atom picture does particularly improve the simulation results, independently on the dihedral potential: the density gets closer to the experimental one, but the value of b side decreases with respect to the experiment (and to the united atom FFs). For CBZ instead the reparametrization of the dihedral seems very relevant: the full atom F score drops from a very poor 0.043 to 0.015 because of that; however, the optimized united atom FFs perform slightly better. For pCBP the comparison is even more rewarding for the united atom force fields, which give scores of about 0.01 versus 0.05-0.06 for the full atom ones, thus confirming the necessity of tailoring the LJ parameters for solid state simulations. Finally, these tests provided us with an estimate of the computational savings brought by the united atom approximation, consisting in an appreciable factor of about six times (0.4 days/ns vs 2.5 days/ns for pCBP on a single logical core of an Intel Xeon E5-2620v2 2.1GHz processor).

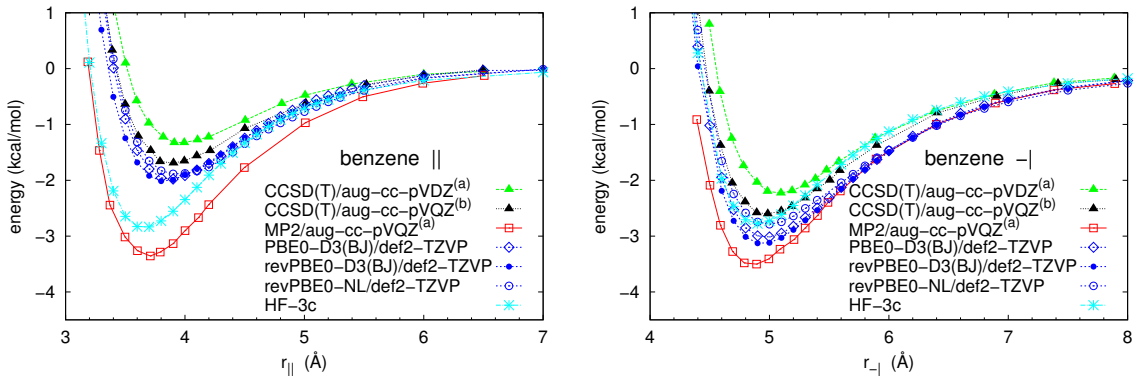

Figure 4: Calculated intermolecular energies for two cofacial (left) and "T" oriented (right) benzene molecules. MP2 and CCSD(T) data are extracted from reference.[89] (a) Counterpoise corrected values; (b) values estimated from counterpoise corrected CCSD(T)/aug-cc-pVDZ and MP2/aug-cc-pVDZ calculations.

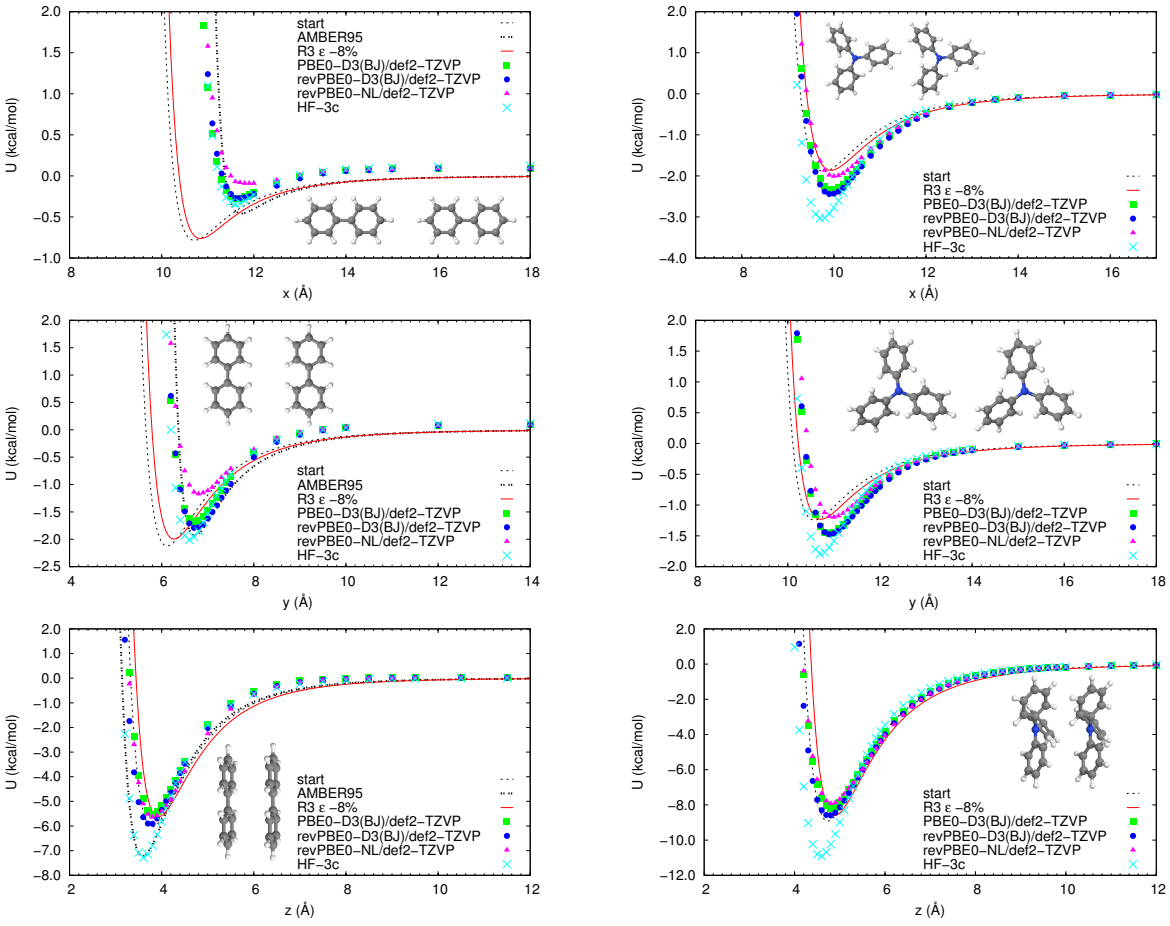

Figure 5: Calculated intermolecular energies for two parallel biphenyl molecules displaced along their x, y and z inertia axes (left), and corresponding energies for two triphenylamine molecules (right).

7 Conclusions

In summary, we derived a simple molecular mechanics force field, aimed at the accurate and computationally efficient simulation of the morphology of materials used in the realization of organic light-emitting diodes. To increase the awareness of the potential users, we would like to recap here the main approximations, limitations, and good practices for a safe application of the force field parameters:

- the force field relies on the united atom approximation, where hydrogen are only implicitely accounted for: this grants a speed-up of about 600%, but also a lack of accuracy in describing specific contacts (see Figure 5), and cannot be used for hydrogen-bond forming systems.

- DFT calculations at the PBE0-D3(BJ)/def2-TZVP level were performed for the parameterization of the point charges on each united atom center, and for the soft torsional potentials between rigid aromatic units: similar calculations are required for any new compound to be studied.

- The Lennard-Jones parameters were empirically optimized in order to maximize the agreement with available experimental data, namely crystal cell shape and size, and the melting temperatures, for a training set of eight compounds.

- As the main empirical tuning of the parameters was performed to match the experimental crystal - hence a solid phase - we hypothesize that the parameterization will be effective also in reproducing another solid phase, the glassy one typically found in OLED devices.

- It is probably impossible to obtain a classical and simple force field "for all seasons" [93]- for instance, coarse-grained force fields for polymers work only close to the temperature and pressure they are derived,[94] and different force fields are required to reproduce high and low pressure benzene polymorphs.[95] In our specific case, reproduction of the

boiling point is not satisfactory, consequently we disencourage the application of the force field for simulations of bulk liquid phases.

- The transferability of the force field was demonstrated by performing the simulation in crystal phase of two compounds outside the training set, which were again in good agreement with experiment. This result, although promising, is not sufficient to ensure the transferability to other compounds, in particular if containing new chemical moieties. In that case, the best practice would be to benchmark again the force field against the experimental crystal structure, if available, or versus any other experimental data.

Having listed all the limitations of the proposed methodology, it also is worth stressing that the good reproduction of physical properties in the solid state, together with the large computational saving expected with respect to full atom force fields, make the force field presented here a suitable candidate for the simulation of the morphology of emissive layers for OLED materials consisting of some thousands of molecules, paving the way towards the their computational screening in a multi-scale approach.

Acknowledgement

This work was supported by the Samsung Advanced Institute of Technology (SAIT)s Global Research Outreach (GRO) Program. The research in Bordeaux has been funded by the French national grant ANR-10-LABX-0042-AMADEus managed by the National Research Agency under the initiative of excellence IdEx Bordeaux programme (reference ANR-10-IDEX-0003-02). The work in Mons was supported by the Programme d'Excellence de la Région Wallonne (OPTI2MAT project) and FNRS-FRFC.

Supporting Information Available

Additional figures: S1) effect of scaling the Lennard-Jones ϵ parameters on the scoring function, S2) compound-wise performances of the different parameterizations, S3) intermolecular

potential energy curves for PCB. S4) torsional energy profiles for NPD and TPBI specific dihedral angles. S5) Glass transition temperature determination for the target compounds S6) Example of the characterization of the crystal-liquid phase transition. Tables with fit parameters of benzene, BPH, PCZ, and TPA intermolecular energies with Morse equation. Table of calculated surface energies for crystalline and glassy samples. Archive containing: CHARMM topology and parameter files (united atom R3 $\epsilon 8\%$ and full atom T-FA), typical NAMD configuration file, pdb files for united atom and full atom crystal cells. This material is available free of charge via the Internet at `http://pubs.acs.org/`.

Notes and References

(1) Boudreault, P.-L. T.; Beaupre, S.; Leclerc, M. *Polym. Chem.* **2010**, *1*, 127–136.

(2) Gendron, D.; Leclerc, M. *Energy Environ. Sci.* **2011**, *4*, 1225–1237.

(3) Barito, A.; Sykes, M. E.; Huang, B.; Bilby, D.; Frieberg, B.; Kim, J.; Green, P. F.; Shtein, M. *Adv. Ener. Mater.* **2014**, *4*, 1400216.

(4) Mishra, A.; Fischer, M. K. R.; Bäuerle, P. *Angew. Chem. Int. Ed.* **2009**, *48*, 2474–2499.

(5) Yeh-Yung Lin, R.; Lin, H.-W.; Yen, Y.-S.; Chang, C.-H.; Chou, H.-H.; Chen, P.-W.; Hsu, C.-Y.; Chen, Y.-C.; Lin, J. T.; Ho, K.-C. *Energy Environ. Sci.* **2013**, *6*, 2477–2486.

(6) Zhou, N.; Lee, B.; Timalsina, A.; Guo, P.; Yu, X.; Marks, T. J.; Facchetti, A.; Chang, R. P. H. *J. Phys. Chem. C* **2014**, *118*, 16967–16975.

(7) Yook, K. S.; Lee, J. Y. *Adv. Mater.* **2014**, *26*, 4218–4233.

(8) Chen, D.; Su, S.-J.; Cao, Y. *J. Mater. Chem.* **2014**, *2*, 9565–9578.

(9) Zhang, T.; Chu, B.; Li, W.; Su, Z.; Peng, Q. M.; Zhao, B.; Luo, Y.; Jin, F.; Yan, X.; Gao, Y.; Wu, H.; Zhang, F.; Fan, D.; Wang, J. *ACS Appl. Mater. Interfaces* **2014**, *6*, 11907–11914.

(10) He, X.; Cai, D.; Kang, D.-Y.; Haske, W.; Zhang, Y.; Zuniga, C. A.; Wunsch, B. H.; Barlow, S.; Leisen, J.; Bucknall, D.; Kippelen, B.; Marder, S. R. *J. Mater. Chem. C* **2014**, *2*.

(11) Gaj, M. P.; Fuentes-Hernandez, C.; Zhang, Y.; Marder, S. R.; Kippelen, B. *Org. Electron.* **2015**, *16*, 109 – 112.

(12) Suzuki, Y.; Zhang, Q.; Adachi, C. *J. Mater. Chem. C* **2015**, *3*, 1700–1706.

(13) Mayr, C.; Lee, S. Y.; Schmidt, T. D.; Yasuda, T.; Adachi, C.; Brütting, W. *Adv. Funct. Mater.* **2014**, *24*, 5232–5239.

(14) Gong, Y.; Liu, J.; Zhang, Y.; He, G.; Lu, Y.; Fan, W. B.; Yuan, W. Z.; Sun, J. Z.; Zhang, Y. *J. Mater. Chem.* **2014**, *2*, 7552–7560.

(15) Huang, J.; Sun, N.; Yang, J.; Tang, R.; Li, Q.; Ma, D.; Li, Z. *Adv. Funct. Mater.* **2014**, *24*, 7645–7654.

(16) Chen, L.; Jiang, Y.; Nie, H.; Hu, R.; Kwok, H. S.; Huang, F.; Qin, A.; Zhao, Z.; Tang, B. Z. *ACS Appl. Mater. Interfaces* **2014**, *6*, 17215–17225.

(17) Choi, E. Y.; Mazur, L.; Mager, L.; Gwon, M.; Pitrat, D.; Mulatier, J. C.; Monnereau, C.; Fort, A.; Attias, A. J.; Dorkenoo, K.; Kwon, J. E.; Xiao, Y.; Matczyszyn, K.; Samoc, M.; Kim, D.-W.; Nakao, A.; Heinrich, B.; Hashizume, D.; Uchiyama, M.; Park, S. Y.; Mathevet, F.; Aoyama, T.; Andraud, C.; Wu, J. W.; Barsella, A.; Ribierre, J. C. *Phys. Chem. Chem. Phys.* **2014**, *16*, 16941–16956.

(18) Yook, K. S.; Lee, J. Y. *Adv. Mater.* **2012**, *24*, 3169–3190.

(19) Baumeier, B.; May, F.; Lennartz, C.; Andrienko, D. *J. Mater. Chem.* **2012**, *22*, 10971–10976.

(20) Kordt, P.; van der Holst, J. J. M.; Al Helwi, M.; Kowalsky, W.; May, F.; Badinski, A.; Lennartz, C.; Andrienko, D. *Adv. Funct. Mater.* **2015**, *25*, 1955–1971.

(21) Perucco, B.; Reinke, N.; Rezzonico, D.; Knapp, E.; Harkema, S.; Ruhstaller, B. *Org. Electron.* **2012**, *13*, 1827 – 1835.

(22) Mesta, M.; Carvelli, M.; de Vries, R. J.; van Eersel, H.; van der Holst, J. J. M.; Schober, M.; Furno, M.; Lüssem, B.; Leo, K.; Loebl, P.; Coehoorn, R.; Bobbert, P. A. *Nat. Mater.* **2013**, *12*, 652–658.

(23) van Eersel, H.; Bobbert, P. A.; Janssen, R. A. J.; Coehoorn, R. *Appl. Phys. Lett.* **2014**, *105*, 143303.

(24) Neumann, T.; Danilov, D.; Lennartz, C.; Wenzel, W. *J. Comput. Chem.* **2013**, *34*, 2716–2725.

(25) Ratcliff, L. E.; Grisanti, L.; Genovese, L.; Deutsch, T.; Neumann, T.; Danilov, D.; Wenzel, W.; Beljonne, D.; Cornil, J. *J. Chem. Theory Comput.* 10.1021/acs.jctc.5b00057.

(26) Mackerell, A. D. *J. Comput. Chem.* **2004**, *25*, 1584–1604.

(27) Kwiatkowski, J. J.; Nelson, J.; Li, H.; Bredas, J. L.; Wenzel, W.; Lennartz, C. *Phys. Chem. Chem. Phys.* **2008**, *10*, 1852–1858.

(28) Lukyanov, A.; Lennartz, C.; Andrienko, D. *Phys. Status Solidi (a)* **2009**, *206*, 2737–2742.

(29) May, F.; Al-Helwi, M.; Baumeier, B.; Kowalsky, W.; Fuchs, E.; Lennartz, C.; Andrienko, D. *J. Am. Chem. Soc.* **2012**, *134*, 13818–13822.

(30) Friederich, P.; Symalla, F.; Meded, V.; Neumann, T.; Wenzel, W. *J. Chem. Theory Comput.* **2014**, *10*, 3720–3725.

(31) Tao, Y.; Yuan, K.; Chen, T.; Xu, P.; Li, H.; Chen, R.; Zheng, C.; Zhang, L.; Huang, W. *Adv. Mater.* **2014**, *26*, 7930–7930.

(32) Adachi, C. *Jpn. J. Appl. Phys.* **2014**, *53*, 060101.

(33) Jankus, V.; Data, P.; Graves, D.; McGuinness, C.; Santos, J.; Bryce, M. R.; Dias, F. B.; Monkman, A. P. *Adv. Funct. Mater.* **2014**, *24*, 6178–6186.

(34) Moral, M.; Muccioli, L.; Son, W.-J.; Olivier, Y.; Sancho-García, J. C. *J. Chem. Theory Comput.* **2015**, *11*, 168–177.

(35) Yu, M.; Wang, S.; Shao, S.; Ding, J.; Wang, L.; Jing, X.; Wang, F. *J. Mater. Chem. C* **2015**, *3*, 861–869.

(36) Yuan, W. Z.; Gong, Y.; Chen, S.; Shen, X. Y.; Lam, J. W. Y.; Lu, P.; Lu, Y.; Wang, Z.; Hu, R.; Xie, N.; Kwok, H. S.; Zhang, Y.; Sun, J. Z.; Tang, B. Z. *Chem. Mater.* **2012**, *24*, 1518–1528.

(37) Chemical drawings were generated by ChemSpider http://www.chemspider.com Accessed date 04/20/2015.

(38) Sasabe, H.; Kido, J. *Chem. Mater.* **2011**, *23*, 621–630.

(39) Muccioli, L.; D'Avino, G.; Berardi, R.; Orlandi, S.; Pizzirusso, A.; Ricci, M.; Roscioni, O. M.; Zannoni, C. In *Multiscale Modelling of Organic and Hybrid Photovoltaics*; Beljonne, D., Cornil, J., Eds.; Top. Curr. Chem.; Springer Berlin Heidelberg, 2014; Vol. 352; pp 39–101.

(40) In this work, we enforced the united atom approximation also to the hydrogen attached to carbazole (CBZ) nitrogen (NH atom type in Table 1). This choice prevents the formation of a hydrogen bond: we discourage then the adoption of our force field for carbazole in presence of hydrogen bond acceptors.

(41) Tiberio, G.; Muccioli, L.; Berardi, R.; Zannoni, C. *ChemPhysChem* **2009**, *10*, 125–136.

(42) Vanommeslaeghe, K.; Hatcher, E.; Acharya, C.; Kundu, S.; Zhong, S.; Shim, J.; Darian, E.; Guvench, O.; Lopes, P.; Vorobyov, I.; Mackerell, A. D. *J. Comput. Chem.* **2010**, *31*, 671–690.

(43) Cornell, W. D.; Cieplak, P.; Bayly, C. I.; Gould, I. R.; Merz Jr., K. M.; erguson, D. M. F.; Spellmeyer, D. C.; Fox, T.; Caldwell, J. W.; Kollman, P. A. *J. Am. Chem. Soc.* **1995**, *117*, 5179.

(44) Pizzirusso, A.; Di Pietro, M. E.; De Luca, G.; Celebre, G.; Longeri, M.; Muccioli, L.; Zannoni, C. *ChemPhysChem* **2014**, *15*, 1356–1367.

(45) Reva, I.; Lapinski, L.; Chattopadhyay, N.; Fausto, R. *Phys. Chem. Chem. Phys.* **2003**, *5*, 3844–3850.

(46) Hénin, J.; Chipot, C. *J. Chem. Phys.* **2004**, *121*, 2904–2914.

(47) Weiner, S. J.; Kollmann, P. A.; Case, D. A.; Singh, U. C.; Ghio, C.; Alagona, G.; Profeta, S.; Weiner, P. *J. Am. Chem. Soc.* **1984**, *106*, 765–784.

(48) Yang, L. J.; Tan, C. H.; Hsieh, M. J.; Wang, J. M.; Duan, Y.; Cieplak, P.; Caldwell, J.; Kollman, P. A.; Luo, R. *J. Phys. Chem. B* **2006**, *110*, 13166–13176.

(49) von Lilienfeld, O. A.; Andrienko, D. *J. Chem. Phys.* **2006**, *124*, 054307.

(50) Wang, J.; Wolf, R. M.; Caldwell, J. W.; Kollman, P. A.; Case, D. A. *J. Comput. Chem.* **2004**, *25*, 1157.

(51) Perdew, J. P.; Ernzerhof, M.; Burke, K. *J. Chem. Phys.* **1996**, *105*, 9982.

(52) Perdew, J. P.; Burke, K.; Ernzerhof, M. *Phys. Rev. Lett.* **1996**, *77*, 3865–3868.

(53) Zhang, Y.; Yang, W. *Phys. Rev. Lett.* **1998**, *80*, 890.

(54) Adamo, C.; Barone, V. *J. Chem. Phys.* **1999**, *110*, 6158–6170.

(55) Weigend, F.; Ahlrichs, R. *Phys. Chem. Chem. Phys.* **2005**, *7*, 3297–3305.

(56) Grimme, S.; Ehrlich, S.; Goerigk, L. *J. Comput. Chem.* **2011**, *32*, 1456–1465.

(57) Besler, B. H.; Merz Jr, K. M.; Kollman, P. A. *J. Comput. Chem.* **1990**, *11*, 431–439.

(58) Frisch, M. J.; Trucks, G. W.; Schlegel, H. B.; Scuseria, G. E.; Robb, M. A.; Cheeseman, J. R.; Scalmani, G.; Barone, V.; Mennucci, B.; Petersson, G. A.; Nakatsuji, H.; Caricato, M.; Li, X.; Hratchian, H. P.; Izmaylov, A. F.; Bloino, J.; Zheng, G.; Sonnenberg, J. L.; Hada, M.; Ehara, M.; Toyota, K.; Fukuda, R.; Hasegawa, J.; Ishida, M.; Nakajima, T.; Honda, Y.; Kitao, O.; Nakai, H.; Vreven, T.; Montgomery, J. A., Jr.; Peralta, J. E.; Ogliaro, F.; Bearpark, M.; Heyd, J. J.; Brothers, E.; Kudin, K. N.; Staroverov, V. N.; Kobayashi, R.; Normand, J.; Raghavachari, K.; Rendell, A.; Burant, J. C.; Iyengar, S. S.; Tomasi, J.; Cossi, M.; Rega, N.; Millam, J. M.; Klene, M.; Knox, J. E.; Cross, J. B.; Bakken, V.; Adamo, C.; Jaramillo, J.; Gomperts, R.; Stratmann, R. E.; Yazyev, O.; Austin, A. J.; Cammi, R.; Pomelli, C.; Ochterski, J. W.; Martin, R. L.; Morokuma, K.; Zakrzewski, V. G.; Voth, G. A.; Salvador, P.; Dannenberg, J. J.; Dapprich, S.; Daniels, A. D.; Farkas,; Foresman, J. B.; Ortiz, J. V.; Cioslowski, J.; Fox, D. J. Gaussian09 Revision A.01. Gaussian Inc. Wallingford CT 2009.

(59) Neese, F. *Wiley Interdiscip. Rev.-Comput. Mol. Sci.* **2012**, *2*, 73–78.

(60) Phillips, J. C.; Braun, R.; Wang, W.; Gumbart, J.; Tajkhorshid, E.; Villa, E.; Chipot, C.; Skeel, R. D.; Kale, L.; Schulten, K. *J. Comput. Chem.* **2005**, *26*, 1781–1802.

(61) The atom types CW and N5 were introduced to identify proper and improper dihedrals of PTBI. Apart this, they coincide with CY and N4 atom types.

(62) Charbonneau, G. P.; Delugeard, Y. *Acta Crystallogr. Sect. B* **1977**, *33*, 1586–1588.

(63) Gerkin, R. E.; Reppart, W. J. *Acta Crystallogr. Sect. C* **1986**, *42*, 480–482.

(64) Belsky, V. K.; Zavodnik, V. E.; Vozzhennikov, V. M. *Acta Crystallogr. Sect. C* **1984**, *40*, 1210–1211.

(65) Sun, Y.-H.; Zhu, X.-H.; Chen, Z.; Zhang, Y.; Cao, Y. *J. Org. Chem.* **2006**, *71*, 6281–6284.

(66) Low, P. J.; Paterson, M. A. J.; Yufit, D. S.; Howard, J. A. K.; Cherryman, J. C.; Tackley, D. R.; Brook, R.; Brown, B. *J. Mater. Chem.* **2005**, *15*, 2304–2315.

(67) Woźniak, K.; Kariuki, B.; Jones, W. *Acta Crystallogr. Sect. C* **1991**, *47*, 1113–1114.

(68) Avendano, C.; Espada, M.; Ocana, B.; Garcia-Granda, S.; Diaz, M.; Tejerina, B.; Gomez-Beltran, F.; Martinez, A.; Elguero, J. *J. Chem. Soc., Perkin Trans. 2* **1993**, 1547–1555.

(69) Sobolev, A. N.; Belsky, V. K.; Romm, I. P.; Chernikova, N. Y.; Guryanova, E. N. *Acta Crystallogr. Sect. C* **1985**, *41*, 967–971.

(70) In the case of a relatively small isotropic box deformation $l_s^i = \lambda\ l_e^i$, or $l_s^i = (1+x)l_e^i$ with $x = \lambda - 1$ and $|x| << 1$, F becomes approximately equal to $|x|$.
In fact for this particular case $V_s = (1+x)^3 V_e$, $\Delta_{vol} = (1/3)|V_e - V_e(1+x)^3|/V_e = (1/3)|3x+3x^2+x^3|$, and $\Delta_{def} = (1/3)(3|x|+3|x|^2+3|x|^3)$. For small $|x|$ hence we have Δ_{vol} and $\Delta_{def} \simeq |x|$, and of course $F = 1/2(\Delta_{vol} + \Delta_{def}) \simeq |x|$.

(71) D'Avino, G.; Muccioli, L.; Zannoni, C.; Beljonne, D.; Soos, Z. G. *J. Chem. Theory Comput.* **2014**, *10*, 4959–4971.

(72) Jurečka, P.; Černý, J.; Hobza, P.; Salahub, D. R. *J. Comput. Chem.* **2007**, *28*, 555–569.

(73) Grimme, S. *WIREs Comput. Mol. Sci.* **2011**, *1*, 211–228.

(74) Sherrill, C. D. *Acc. Chem. Res.* **2013**, *46*, 1020–1028.

(75) Sherrill, C. D.; Sumpter, B. G.; Sinnokrot, M. O.; Marshall, M. S.; Hohenstein, E. G.; Walker, R. C.; Gould, I. R. *J. Comput. Chem.* **2009**, *30*, 2187–2193.

(76) Olivier, Y.; Muccioli, L.; Zannoni, C. *ChemPhysChem* **2014**, *15*, 1345–1355.

(77) Pettersson, I.; Liljefors, T. *J. Comput. Chem.* **1987**, *8*, 1139–1145.

(78) Jorgensen, W. L.; Tirado-Rives, J. *J. Am. Chem. Soc.* **1988**, *110*, 1657–1666.

(79) Olivier, Y.; Muccioli, L.; Lemaur, V.; Geerts, Y. H.; Zannoni, C.; Cornil, J. *J. Phys. Chem. B* **2009**, *113*, 14102–14111.

(80) D'Avino, G.; Mothy, S.; Muccioli, L.; Zannoni, C.; Wang, L.; Cornil, J.; Beljonne, D.; Castet, F. *J. Phys. Chem. C* **2013**, *117*, 12981–12990.

(81) Agrawal, P. M.; Rice, B. M.; Thompson, D. L. *J. Chem. Phys.* **2003**, *118*, 9680–9688.

(82) Zhang, Y.; Maginn, E. J. *J. Chem. Phys.* **2012**, *136*, 144116.

(83) Marcon, V.; Raos, G. *J. Am. Chem. Soc.* **2006**, *128*, 1408–1409.

(84) Massaro, F. R.; Moret, M.; Bruno, M.; Aquilano, D. *Cryst. Growth & Des.* **2013**, *13*, 1334–1341.

(85) Rohl, A.; Gay, D. *J. Cryst. Growth* **1996**, *166*, 84 – 90.

(86) Experimental melting points were obtained from Sigma Aldrich online catalogue http://www.sigmaaldrich.com/catalog/ Accessed date 04/20/2015.

(87) Vydrov, O. A.; Van Voorhis, T. *J. Chem. Phys.* **2010**, *133*, 244103.

(88) Sure, R.; Grimme, S. *J. Comput. Chem.* **2013**, *34*, 1672–1685.

(89) Sinnokrot, M. O.; Sherrill, C. D. *J. Phys. Chem. A* **2004**, *108*, 10200–10207.

(90) Yang, J.; Hu, W.; Usvyat, D.; Matthews, D.; Schtz, M.; Chan, G. K.-L. *Science* **2014**, *345*, 640–643.

(91) Worle, M.; Losio, P. A.; Gunter, P. *private communication* **2006**, CCDC 298742 REHJAQ01.

(92) Song, W.-F.; Wu, Y.; Fan, Y.; Wang, Y.; Liu, Y. *Acta Crystall. Sect. E* **2009**, *65*, o2461.

(93) Peter, C.; Kremer, K. *Faraday Discuss.* **2010**, *144*, 9–24.

(94) Carbone, P.; Varzaneh, H. A. K.; Chen, X.; Müller-Plathe, F. *J. Chem. Phys.* **2008**, *128*, 064904.

(95) Hofmann, D. W. M.; Kuleshova, L. N. *Cryst. Growth Des.* **2014**, *14*, 3929–3934.

Table of content graphic